Asian Journal of Chemistry; Vol. 37, No. 4 (2025), 817-829

ASIAN JOURNAL OF CHEMISTRY

https://doi.org/10.14233/ajchem.2025.33340

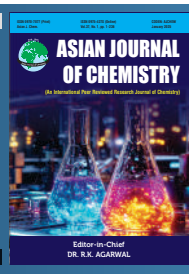

Synthesis, Spectral Characterization and Theoretical Evaluation of Azo-Metal Complexes for Potential Antioxidant and Anticancer Activities

DURGA PRASAD MISHRA[1], PRAFULLA KUMAR SAHU[1,2,*], ASHISH KUMAR SARANGI[3], SUSOVAN BORAT[4], SHUDESNA SARKAR[4] and DEBANJAN SEN[4]

[1]School of Pharmacy and Life Sciences, Centurion University of Technology and Management, Balangir-767001, India
[2]Department of Pharmacy, Keonjhar Institute of Medical Science and Research, Tentulinanda, Dimbo, Keonjhar-758014, India
[3]School of Applied Sciences, Centurion University of Technology and Management, Balangir-767001, India
[4]Department of Pharmaceutical Chemistry, B.C.D.A. College of Pharmacy & Technology, Kolkata-700127, India

*Corresponding author: E-mail: kunasahu1@gmail.com

Received: 8 January 2025; *Accepted*: 24 February 2025; *Published online*: 29 March 2025; AJC-21942

The synthesis and evaluation of azo-metal complexes derived from *m*-aminophenol and 2,4-dihydroxyacetophenone were conducted to investigate their antioxidant and anticancer potential. Ligand, 3-(2′,4′-dihydroxy-5-acetylphenylazo)-1-hydroxybenzene (LH_2) was synthesized and complexed with Cu(II), Ni(II), Co(II) and Zn(II) ions. The compounds were characterized with different spectroscopic methods, including FTIR, ^{1}H NMR, ^{13}C NMR, ESR, ESI-MS and XRD, along with thermal analysis (TGA/DTA) and SEM-EDS. Antioxidant activity assessed through the DPPH assay revealed that Cu(II) complex showed the highest radical scavenging activity with an IC_{50} of 13.38 µg/mL, outperforming the free ligand (IC_{50} = 34.57 µg/mL). Anticancer activity was evaluated against MCF-7 (breast cancer cell line) and HepG2 (liver cancer cell line) cell lines using the MTT assay. Ni(II) and Co(II) complexes demonstrated superior cytotoxicity with IC_{50} values of 13.48 µg/mL and 14.42 µg/mL, respectively, at 48 h, compared to the standard drug doxorubicin (IC_{50} = 10.31 µg/mL). Molecular docking studies against 17-β-HSD1 indicated strong binding affinities, particularly for Ni(II) complex (-9.81 kcal/mol), attributed to favourable coordination and electronic properties. Computational analyses, including molecular dynamics simulations and HOMO-LUMO energy evaluations, highlighted the stability, reactivity and interaction potential of the metal complexes. ADME profiling confirmed their drug-likeness, with Cu(II) and Ni(II) complexes showing promising pharmacokinetic attributes, including high gastrointestinal absorption and blood-brain barrier permeability.

Keywords: Azo-metal complexes, Anticancer study, MD simulation, Docking study, HOMO-LUMO analysis.

INTRODUCTION

Azo dyes are synthetic compounds characterized by the presence of one or more azo groups (-N=N-) linking aromatic rings. Due to their vibrant colours, these dyes have widespread applications in industries such as textiles, food and cosmetics [1]. In the pharmacological field, azo dyes have garnered attention for their potential as bioactive agents. Some azo dyes and their derivatives exhibit antimicrobial, anticancer and antioxidant properties, making them valuable in drug design and development [2]. Additionally, azo dyes are often utilized in the preparation of azo-metal complexes, which have been shown to possess enhanced therapeutic activities, including antimalarial and anti-inflammatory activities. Their versatility as both chromophores and functional groups allows them to be incorporated into various pharmaceutical formulations, enhancing drug delivery and bioactivity. However, their use in medicine requires careful consideration of their safety profile, as some azo compounds can be metabolized into potentially harmful aromatic amines [3].

Aromatic azo dyes have emerged as promising candidates for antioxidant and anticancer therapies, owing to their unique structural attributes and versatile biological activities [4,5]. The presence of the azo linkage in these compounds, coupled with electron-donating or electron-withdrawing substituents on the aromatic rings, significantly influences their redox behaviour, making them effective in scavenging reactive oxygen species (ROS) [6]. Excessive ROS levels are implicated in oxidative

stress, a key factor in the pathogenesis of cancer and other chronic diseases. Azo dyes act as antioxidants by neutralizing free radicals, thereby protecting cellular components such as DNA, proteins and lipids from oxidative damage. This antioxidant activity contributes to their chemopreventive properties, potentially reducing cancer initiation and progression [7]. In the context of anticancer therapy, aromatic azo dyes exhibit cytotoxic effects against various cancer cell lines through multiple mechanisms. They can induce apoptosis, the programmed cell death vital for eliminating cancer cells, by activating caspase pathways or modulating mitochondrial membrane potential. Some azo dyes interact with DNA, leading to the inhibition of topoisomerase enzymes, essential for DNA replication in rapidly dividing cells, thereby halting tumor growth [8]. Additionally, their antioxidant properties may help in mitigating oxidative damage to normal cells during chemotherapy, reducing the side effects of conventional anticancer treatments.

The structural flexibility of azo dyes also allows for functionalization and conjugation with other bioactive molecules, enhancing their specificity and therapeutic efficacy. For instance, metal complexes of azo dyes have shown amplified anticancer activities due to the synergistic effects of the metal ions and the azo scaffold [9]. Furthermore, azo dyes with specific substituents can target cancer cell receptors or be designed as prodrugs that activate selectively within the tumor microenvironment, minimizing off-target effects. While aromatic azo dyes hold significant promise as antioxidant and anticancer agents, their development as drug candidates necessitates thorough investigations into their pharmacokinetics, bioavailability and toxicity [10]. Advancements in the computational modeling and high throughput screening are facilitating the optimization of their design, hence enabling their incorporation into modern treatment approaches.

In this article, the synthesis and characterization of novel azo ligand and its corresponding metal(II) complexes were carried out. The azo ligand, 3-(2′,4′-dihydroxy-5-acetylphenylazo)-1-hydroxybenzene (LH_2), was synthesized from *m*-amino phenol and 2,4-dihydroxyacetophenone under optimized conditions. The characterization of the synthesized azo-ligand and its metal complexes using various spectroscopic techniques including the biological potential was evaluated *in silico* using molecular docking studies and ADME analysis.

EXPERIMENTAL

All reagents used were of analytical grade and purchased from Merck, Sigma-Aldrich and Hi-Media Ltd. The analytical data for hydrogen, carbon and nitrogen were obtained using a Perkin-Elmer 2400 elemental analyzer. FTIR spectral analyses were performed using KBr discs on a Perkin-Elmer Spectrum IR Version 10.6.1 in the 4000–400 cm^{-1} range. The ^1H and ^{13}C NMR spectra were recorded on a Jeol ECZ 400 MHz instrument, with the chemical shifts expressed in parts per million (ppm) relative to TMS. Mass spectrometry analysis was conducted using an ESI-MS on a Waters Xevo G2-XS QTOF mass spectrometer. The EPR spectra were recorded on a Bruker EMX instrument operating in the solid-state X-band at room temperature. Thermal analysis was carried out using a NETZSCH TG 209F1 Libra, with a heating rate of 10 ºC/min, over a temperature range of 0–900 ºC. Powder XRD analyses of the complexes were conducted using a Bruker AXS D8 instrument. The surface morphology of the synthesized compounds was examined using a scanning electron microscope (model: Jeol7610F plus instrument).

Synthesis of ligand: A new azo-ligand was synthesized from *m*-aminophenol (0.01 M, 1.09 g), which was treated with $NaNO_2$ (15 mL) and HCl (10 mL) to obtain diazonium salt. A solution of 2,4-dihydroxyacetophenone (1.1 g) was slowly added at a temperature below freezing to the solution of diazonium salt to obtain 3-(2′,4′-dihydroxy-5-acetylphenylazo)-1-hydroxybenzene (LH_2). The resultant azo dye was then filtered following thorough washing with distilled water and dried (**Scheme-I**). Yield: 87.3%, m.p.: 290-300 ºC. Anal. of $C_{14}H_{12}O_4N_2$ (m.w.

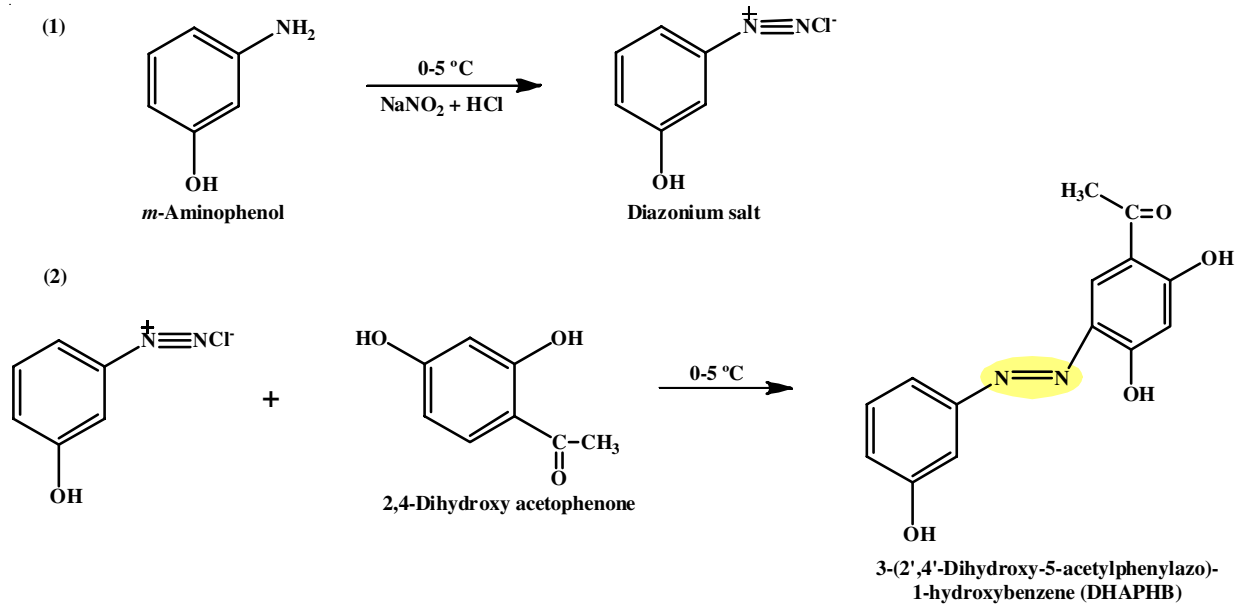

Scheme-I: Synthesis of azodye (LH_2)

272.26): calcd. (found) %: C, 63.31 (63.10); H, 4.37 (4.50); N, 10.21 (10.40). IR (KBr, ν_{max}, cm^{-1}): 1595 (N=N), 1636 (C=O); ^{13}C NMR (400 MHz, DMSO) δ ppm: 98.93 (C1), 105.13, 109.68, 115.44, 129.56, 133.72, 134.08 (Ar–C), 164.37 (C4), 165.03 (C6), 202.79 (C2).

Synthesis of azo-metal complex: An ethanolic solution of azo ligand (LH_2) was mixed with the respective metal(II) salts in a 1:2 molar ratio and refluxed for 1 h at 50-60 ºC. Subsequently, conc. NH_4OH solution was added with continuous stirring until the pH stabilized at approximately 7. The precipitate that obtained was then separated, washed with deionized water and dried under vacuum (**Scheme-II**).

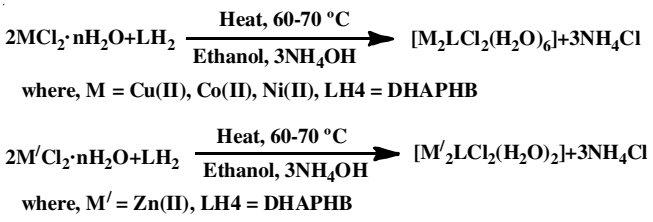

Scheme-II: Synthesis of metal complexes

$[Cu_2LCl_2(H_2O)_6]$: Yield: 92.7%; Deep green, m.p.: 285-295 ºC. Anal. of m.f.: $C_{14}H_{22}O_9N_2Cl_2Cu_2$ (m.w. 560.33): calcd. found (%): C, 31.70 (31.40); H, 3.70 (3.30); N, 4.70 (4.80); Cl, 6.40 (6.50); Cu, 22.30 (22.70); IR (KBr, ν_{max}, cm^{-1}): 1607 ν(C=O), 557 (M–O), 490 (M–N), 1591 ν(-N=N-).

$[Ni_2LCl_2(H_2O)_6]$: Yield: 90.4%; faint green, m.p.: >240 ºC. Anal. of $C_{14}H_{22}O_9N_2Cl_2Ni_2$ (m.w. 550.62): calcd. (found) %: C, 32.30 (21.35); H, 3.60 (3.55); N, 5.10 (5.40); Cl 6.30 (6.63); Ni, 21.0 (21.31); IR (KBr, ν_{max}, cm^{-1}): 1602 (C=O), 581 (M–O), 455 (M–N), 1565 (-N=N-).

$[Co_2LCl_2(H_2O)_6]$: Yield: 88.2%; brown, m.p.: >250 ºC. Anal. of $C_{14}H_{22}O_9N_2Cl_2Co_2$ (m.w. 551.1): calcd. (found) %: C, 34.32 (31.95); H, 3.70 (3.36); N, 5.37 (5.63); Cl, 6.33 (6.15); Co, 21.12 (21.53); IR (KBr, ν_{max}, cm^{-1}): 1616 (C=O), 570 (M–O), 421 (M–N), 1572 (-N=N-),

$[Zn_2LCl_2(H_2O)_2]$: Yield: 85.8%; brown, m.p.: >235 ºC. Anal. of $C_{14}H_{14}O_5N_2Cl_2Zn_2$ (m.w. 491.93): calcd. (found) %: C, 36.13 (35.61); H, 2.73 (2.16); N, 5.63 (5.27); Cl, 7.29 (5.26); Zn, 26.22 (26.32); IR (KBr, ν_{max}, cm^{-1}): 1619 (C=O), 561 (M–O), 497 (M–N), 1591 (-N=N-).

***In vitro* anticancer activity:** The methodology established by Skehan *et al*. [11] was applied to evaluate the capacity of the metal(II) complexes to evaluate its cytotoxicity. Before treatment, the cancer cells were attached to 96-well plates at a density of 10^{-4} cells per well. The complexes were treated in triplicate at varying doses (0, 5, 12.5, 25, 50 and 100 µg/mL) to wells with a cell monolayer. The cells were treated with the synthesized compounds for 48 h at 37 ºC in a 5% CO_2 environment [12]. Subsequent to the incubation period, the cells were fixed, washed and stained utilizing sulforhodamine B (SRB) dye. Acetic acid effectively removed most pigments, while the residual stains were solubilized in Tris-EDTA buffer [13]. The optical density (OD) measurements at 564 nm were conducted utilizing an ELISA microplate reader equipped with automated background absorbance removal. The average absorbance for each concentration was calculated and a dose-response curve was constructed to assess the survival rate of the breast cancer cell line at each concentration [14]. The IC_{50} values, indicating the concentration required to inhibit 50% of cellular proliferation, were determined for the azo dye and its metal(II) complex utilizing the MCF7 and HePG2 cell lines. The cell proliferation was measured with the MTT assay, a colorimetric technique. The kit contains adequate reagents for 192 tests in 24-well plates or 960 assays in 96-well plates [15]. The complexes were individually produced for each dosage and delivered at varying concentrations *viz*. 1, 5, 10, 20, 30 and 50 µg/mL to triplicate wells of the cell monolayer. The cells were grown with the complexes in a 5% CO atmosphere at 37 ºC for 48 h. Subsequent to incubation, the cells were fixed, washed and stained using PBS [16]. To excess stain was removed using acetic acid and the bound stain was eluted with Tris-EDTA buffer. The optical density (OD) measurements at 564 nm were accurately acquired for each well utilizing a cutting-edge ELISA microplate reader with automated background absorbance correction. The mean OD values for each dosage level of the drug were meticulously computed [17]. A survival curve for the breast tumour cell line was constructed by connecting the survival fraction with the drug concentration for each complex. The IC_{50} values provides essential information about the quantity of the azo dye and its metal(II) complexes required to reduce cellular proliferation by 50% [18]. The experiment was performed twice with the MCF7 and HePG2 cell lines. The percentage of cell viability was estimated using the following formula:

$$\text{Survival fraction} = \frac{\text{O.D (treated cells)}}{\text{O.D (control cells)}} \times 100$$

The cytotoxic effects of synthesized compounds were assessed on MCF 7 and HePG 2 cell line.

DPPH assay: The antioxidant activity of the synthesized compounds was evaluated using the DPPH free radical assay. Synthesized compounds at different concentrations (5, 10, 15, 20 and 25 µg/mL) in DMSO solvent were prepared and 0.3 mL of each solution was mixed with 2.7 mL of DPPH solution in DMSO. At room temperature, the mixtures were incubated for 60 min, shielded from light. Radical scavenging activity was then accessed by measuring the absorbance at 517 nm with a UV-Vis spectrophotometer [19]. All the measurements were averaged from three independent replicates for each concentration. Ascorbic acid served as the standard (positive control) and the antioxidant activity was calculated using the following formula:

$$\text{RSA } (\%) = \frac{\text{OD control} - \text{OD sample}}{\text{OD control}} \times 100$$

where OD control refers to the absorbance of the control solution and the OD sample represents the absorbance of the solution containing the test compound. The IC_{50} values for each synthesized compound and the standard was determined by plotting the percentage of DPPH scavenging activity against the sample concentration.

MD simulations: Desmond-2022 software was employed to perform molecular dynamics simulations to study the dynamic

behaviour of the protein-ligand complex. Initial molecular structures were created using Maestro LigPrep software, using topology and the OPLS4 force field, respectively. The OPLS4 force field was used to represent the interactions of the system accurately. The solvated system was energy-minimized to remove steric conflicts, then equilibrated with NPT and NVT ensembles to replicate varied thermodynamic circumstances [20]. A 100 ns MD simulation was performed first, followed by MMPBSA calculations to estimate binding free energy and various analyses to assess structural integrity and dynamic characteristics. The system containing the target biomolecule (*e.g.* protein) and any interacting ligands, ions or cofactors must be prepared before the MD simulation may begin. The protein structure (usually obtained from the Protein Data Bank, PDB) is pre-processed to include missing atoms or side chains, assign protonation states and optimize hydrogen bonds. The protein or molecular complex is subsequently solvated, usually with the TIP3P water model, in a water box. To make sure the system is big enough to prevent edge effects, a buffer is used. Counter ions (*e.g.* Na^+ or Cl^-) were added to neutralize the charge of the system [21]. In some cases, salt concentration (*e.g.* 0.15 M NaCl) was added to replicate the physiological conditions. Desmond uses force fields such as OPLS4, which accurately describe interatomic forces for proteins, lipids and small molecules. Before executing the 100 ns simulation, the energy minimization was carried out to eliminate steric constraints and optimize the shape of the system.

This stage reduces the potential energy of the system, resulting in a stable starting position for the MD simulation. The system is gradually equilibrated to achieve the appropriate temperature and pressure. The system was maintained at a fixed quantity of particles, volume and temperature. A typical time step of 100 ns was used and the simulation progresses by updating the atomic positions and velocities. Atomic coordinates and other properties (*e.g.* velocities) were recorded at regular intervals, typically every 100 ns, generating a trajectory file for post-simulation analysis [22].

After the MD run, the trajectory was analyzed to extract insights about molecular behaviour over the 100 ns timescale. To evaluate the temporal stability of the protein structure, comparing the structure of system at each frame to the initial structure. To analyze flexibility and identify regions of the protein that are highly flexible or rigid.

A Desmond molecular dynamics simulation lasting 100 ns provides detailed insights into the structural dynamics and stability of biomolecular systems. It enables the detection of critical molecular events like as conformational changes, ligand binding and interaction patterns during nanosecond to microsecond periods [23]. Desmond's remarkable efficiency allows even complicated systems to be reproduced with precise force fields, offering vital data for drug discovery, protein function investigations and biomolecular research.

Molecular docking: In current drug discovery platform, molecular docking is a one of the crucial computational tools enabling the efficient prediction of binding affinities between potential drug candidates and their biological targets. Based on *in vitro* findings and corroborating evidence from the literature, 17-β-hydroxysteroid dehydrogenase type 1 (17-β-HSD1) was selected as the target enzyme to evaluate the binding efficacy of the synthesized proposed metal-framed ligand structures. For comparative analysis, estradiol benzoate (E2B), a standard drug, was incorporated into each structure [24]. The binding efficacy of these ligands was assessed through a molecular docking study, following established protocols [25]. The proposed the metal-ligand structures were designed using ChemDraw 20 software, while the standard drug, E2B, was retrieved from the PubChem database (PubChem CID: 44456599). All ligand structures were subsequently optimized using the universal force field (UFF) in Avogadro 1.2.0 software to ensure accurate geometric and energetic configurations. The three-dimensional structure of the target protein, 17-β-HSD1, was obtained from the Protein Data Bank (PDB ID: 3HB5).

Molecular docking studies were conducted using AutoDock 4.2 software, adhering to previously established methodologies [26]. For each ligand, ten docking poses were generated and the pose with the least binding energy (most negative binding energy in kcal/mol) was selected as the most favourable and biologically relevant interaction. The binding interactions of the protein-ligand complexes were visualized and analyzed using BIOVIA Discovery Studio (BIOVIA-DSV) to identify key interactions and elucidate the binding mechanisms [25]. This comprehensive approach ensures a robust assessment of the binding efficacy of the proposed ligands, facilitating the identification of promising candidates for further investigation.

HOMO-LUMO surface energy analyses: The highest occupied molecular orbital (HOMO), the lowest unoccupied molecular orbital (LUMO) and their energy gap ($E_{H\text{-}L}$ eV) are critical parameters for understanding the electronic properties, stability and reactivity of therapeutic candidates [27]. Surface energy analyses of these molecular orbitals provide valuable insights into the electron-donating and accepting capabilities, enabling predictions of binding affinity and molecular interactions. These parameters are particularly useful in assessing molecular reactivity, stability and kinetic behaviour, which are essential for evaluating the efficacy of proposed ligands compared to a standard drug such as estradiol benzoate (E2B). In this study, the HOMO-LUMO energy analyses were conducted using the Avogadro-ORCA 1.2.0 software suite [25]. The restricted Hartree-Fock (RHF) model was employed to calculate the electronic energy at a single point, which allowed for precise determinations of orbital energy levels.

RESULTS AND DISCUSSION

A new azo-ligand was synthesized by refluxing an ethanolic solution of *m*-aminophenol and 2,4-dihydroxyacetophenone. The metal(II) complexes were prepared by the reaction of the newly synthesized azo-ligand with corresponding metal(II) salts. The solid metal(II) complexes were partially soluble in mostly common organic solvents but are completely soluble in DMF and DMSO solvents.

FTIR spectral studies: The peaks correspond to the absorption of IR radiation at the specific wavelengths, indicating the presence of particular functional groups. The key FTIR

TABLE-1
FTIR RESULTS OF LH_2 AND METAL COMPLEXES

Compound	ν(-OH) and (-NH)	ν(C=C)	ν(-N=N-)	ν(C-O)	ν(C-O)	ν(C-H)
LH_2	3191.59	1595.31	1454.34	1222.27	1133.20	1368.20
$[Cu_2LCl_2(H_2O)_6]$	3328.19	1591.28	1470.80	1244.66	–	1370.90
$[Ni_2LCl_2(H_2O)_6]$	3337.00	1602.86	1399.98	–	1244.00	2810.40
$[Co_2LCl_2(H_2O)_6]$	3547.91	1695.84	1430.30	1133.20	835.03	3153.61
$[Zn_2LCl_2(H_2O)_2]$	3588.10	1599.28	1400.56	1762.50	1240.79	3131.79

bands of the synthesized LH_2 and its metal(II) complexes are shown in Table-1.

TGA-DTA: Thermal analysis of the synthesized compounds was conducted using TGA and DTA, in the temperature range of 0-900 ºC. Fig. 1 presents the thermal decomposition characteristics of the Co(II) complex, which displays similar behaviour [28]. The Co(II) complex remained constant up to 107.9 ºC; nevertheless, though a mass loss of 4.96% was observed at 125.4 ºC, indicating a removal of six-coordinated water molecules. The anhydrous metal complexes underwent rapid degradation at 322.6 ºC due to the release of a coordinated chlorine atom and the organic component. Decomposition continued steadily until reaching untill 718 ºC as shown by the plateau in the thermogram. Ultimately, a stable metal oxide was produced, accounting for 9.47% of the total weight of the complex. To determine the kinetic parameters, like activation energy (E_a) and the order of reaction (n), the Freeman-Carrol equation [29] was used:

$$-\frac{dw}{dt} = R_T = \frac{Z}{R_H e^{-E_a/RT}} w^n \qquad (1)$$

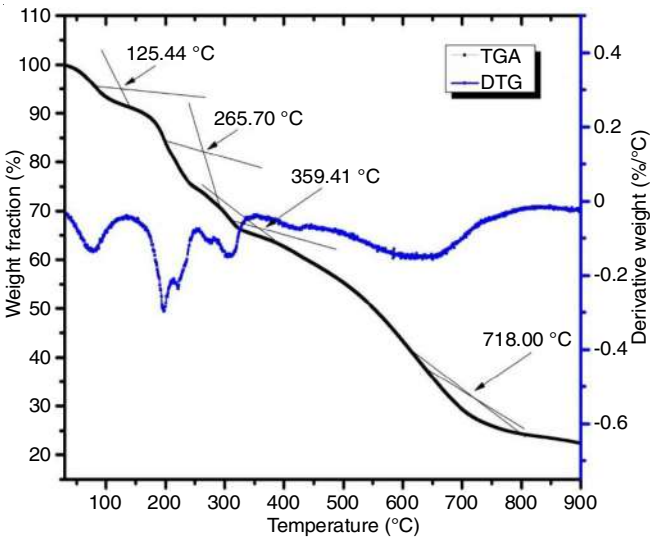

Fig. 1. Thermal analysis of $[Co_2LCl_2(H_2O)_6]$

where the variables RH, W, E_a and Z denote the rate of heating, activation energy and frequency factor, respectively.

$$\Delta \log R_T = n\Delta \log W - \frac{E_a}{2}\cdot 303R\Delta\left(\frac{1}{T}\right) \qquad (2)$$

A plot of Δlog RT *versus* Δlog W shows a relative linearity, where; The value of Δ(1/T) remains set. This plot's slope gives the reaction order (n) and its intercept gives the activation energy (eqn. 2). The reaction order was found to be 0.09748, while the activation energy was determined to be 0.8104 J/mol. The low activation energy value indicates the catalytic effect of metal ions. Moreover, the correlation coefficient (r) of 8.314 matched with the rate of heat degradation observed in the practical results. Table-2 explain thermal analysis of all the metal complexes.

ESR spectral studies: The ESR (X-band) spectrum of Cu(II) complex (Fig. 2) at ambient temperature, yielded g-values of 3.3692, 3.0629, 1.4038 for $g_{\parallel}$, $g_{\perp}$ and g_{av}, respectively [30]. However, the G (axial symmetry) value of 2.40 reveals that within the unit cell, magnetically analogous Cu(II) ions do not

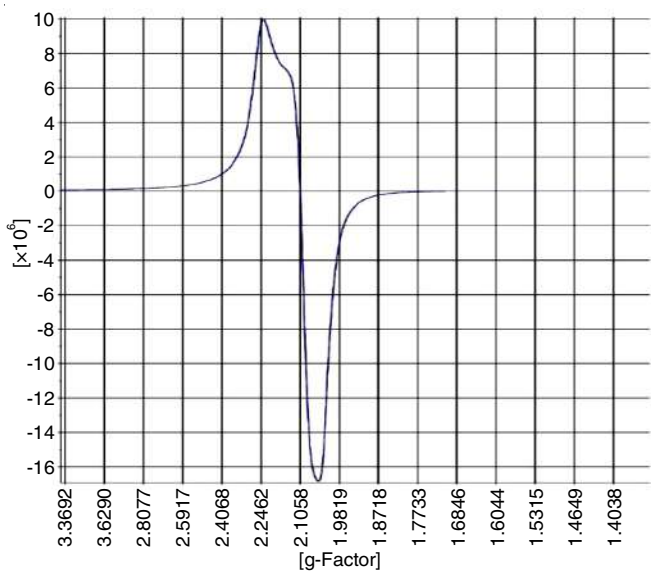

Fig. 2. ESR of $[Cu_2LCl_2(H_2O)_6]$

TABLE-2
TG ANALYSIS OF METAL COMPLEXES

Compounds	Temp. for range of H_2O loss (°C)	Loss of H_2O (%)		Decomposition temperature (°C)	Residue (%)		Residue composition
		Found	Calcd.		Found	Calcd.	
$[Cu_2LCl_2(H_2O)_6]$	115.7	5.12	5.20	325	6.98	7.06	CuO
$[Ni_2LCl_2(H_2O)_6]$	111.3	4.98	5.11	317	7.28	7.39	NiO
$[Co_2LCl_2(H_2O)_6]$	107.9	4.96	5.12	322.6	7.23	7.38	CoO
$[Zn_2LCl_2(H_2O)_2]$	118.6	12.95	13.71	332	5.99	6.06	ZnO

exhibit any exchange interactions. The R (ground state) value of 0.1846 can be explained from the eqn. 3 and the spin-orbit coupling constant (λ) value was derived from eqn. 4.

$$R = g2 - \frac{g1}{g3} - g2 \quad (3)$$

$$g_{avg} = 2\left(1 - \frac{2\lambda}{10Dq}\right) \quad (4)$$

The value of λ, found to be -124.78 cm^{-1}, which was derived from the free ion value (-178.57 cm^{-1}).

^{1}H and ^{13}C NMR spectral studies: The proton resonance spectrum of azo-ligand LH_2 was observed at δ 6.0-7.8 ppm corresponds to the six-phenyl proton whereas a sharp peak at δ 2.5 ppm corresponds to the 3-methyl protons (Fig. 3a). Further a sharp peak was observed at δ 6.2 to δ 7.9 ppm for three different phenolic protons (for *ortho*-, *meta*- and *para*-H). The resonance observed between δ 2.87 and δ 2.98 ppm in Zn(II) complex, with an integration corresponding to 4 protons, was attributed to water molecules coordinated to the metal ion [31] (Fig. 3b). The absence of signals for phenolic protons has been confirmed to facilitate coordination through the deprotonation approach.

For ^{1}H NMR data was further supported by ^{13}C NMR results demonstrating a signal resulting from -CH_3 at δ 26.3 ppm showed in azo-ligand LH_2 (Fig. 4a). Further, a signal attributed to the ketone (>C=O) group was detected at δ 202.7 ppm, whereas >C-O groups was identified at δ 164.3 and δ 165.0 ppm [32]. The signals from the aromatic carbons were observed at δ 100.6 to δ 134.0 ppm.Nevertheless, the phenolic and carboxylic carbon experienced a deshielding effect, suggesting their involvement in interaction with the Zn^{2+} metal ion (Fig. 4b).

Morphological studies: The SEM micrographs of azo-ligand LH_2 and $[Co_2LCl_2(H_2O)_6]$ were recorded at 400 nm and

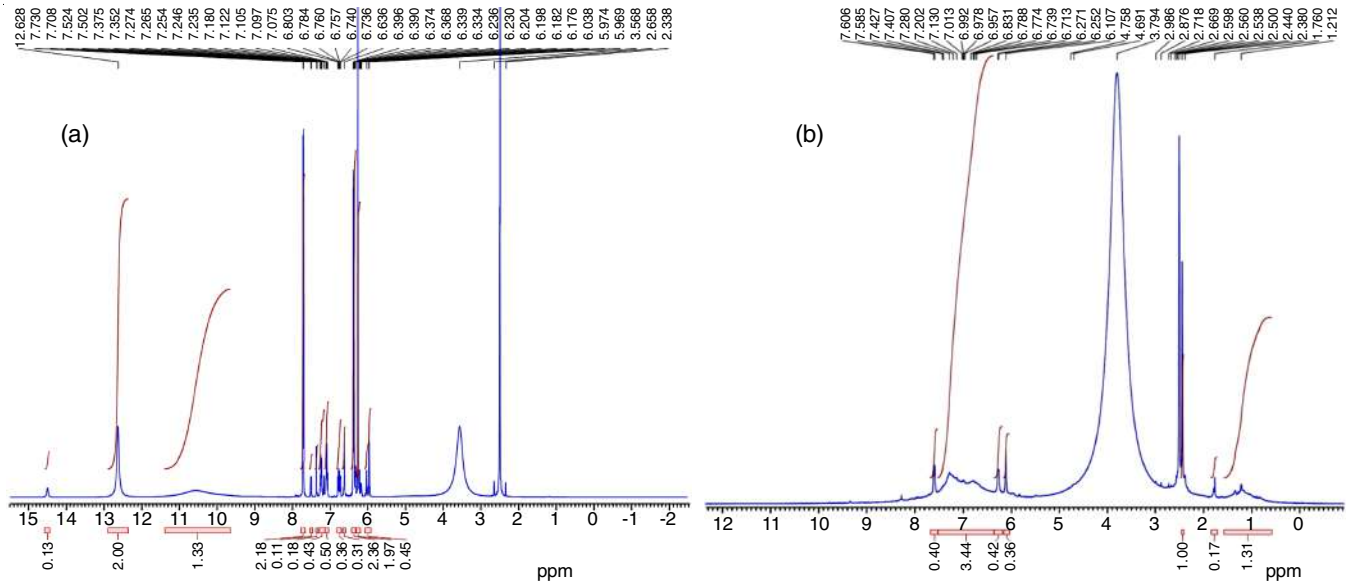

Fig. 3. ^{1}H NMR of (a) LH_2 and (b) $[Zn_2LCl_2(H_2O)_2]$

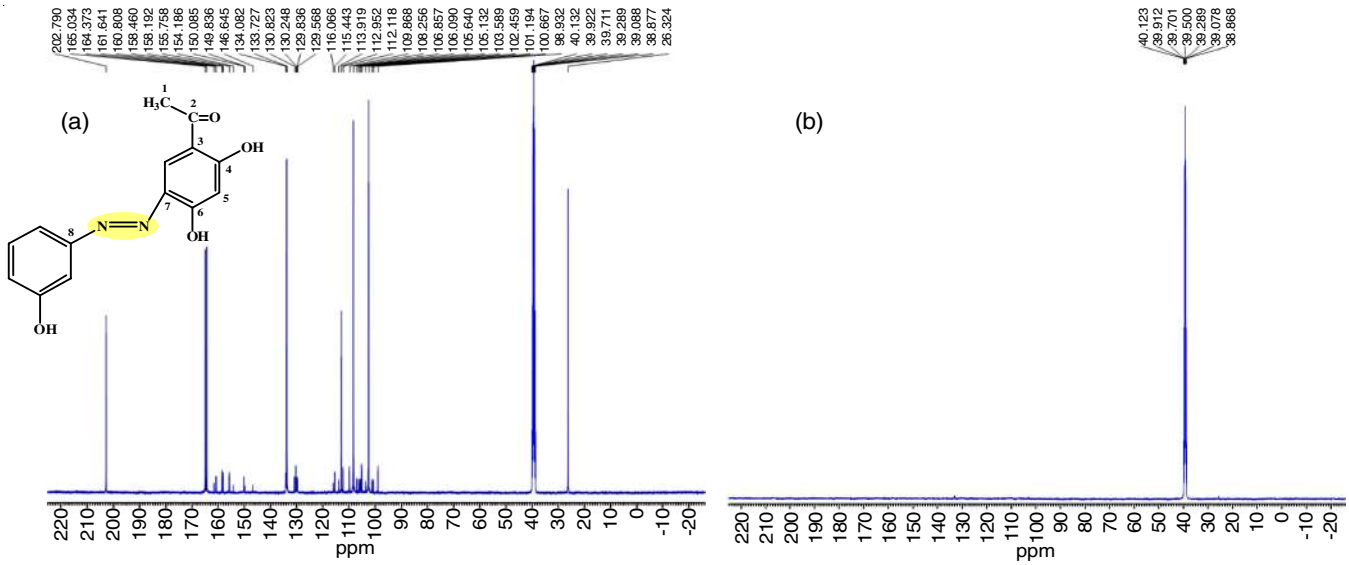

Fig. 4. ^{13}C NMR of (a) LH_2 and (b) $[Zn_2LCl_2(H_2O)_2]$

depict a granular texture. The energy dispersive X-ray (EDS) study of LH_2 and the complex $[Co_2LCl_2(H_2O)_6]$ reveals the existence of elements C, O, Cl and Co [33] (Figs. 5 & 6).

ESI-MS spectral studies: The mass spectra of azo-ligand LH_2 demonstrated *m/z* 230.06 due to the immediate loss of acetyl group, congruent with its molecular mass (Fig. 7a). The peak

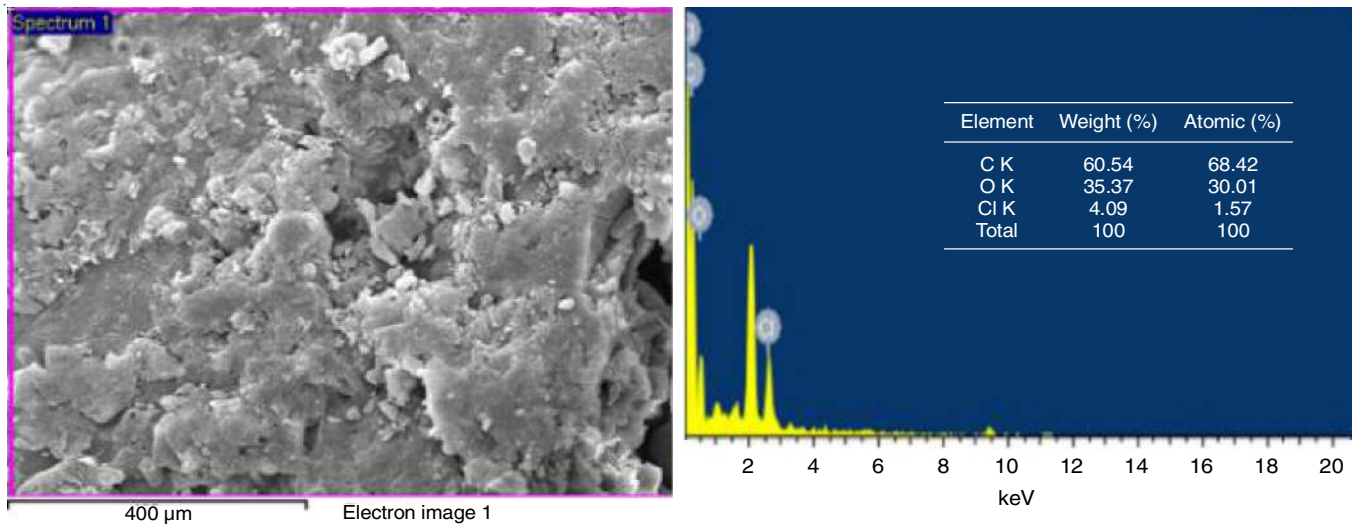

Fig. 5. SEM and EDS of LH_2

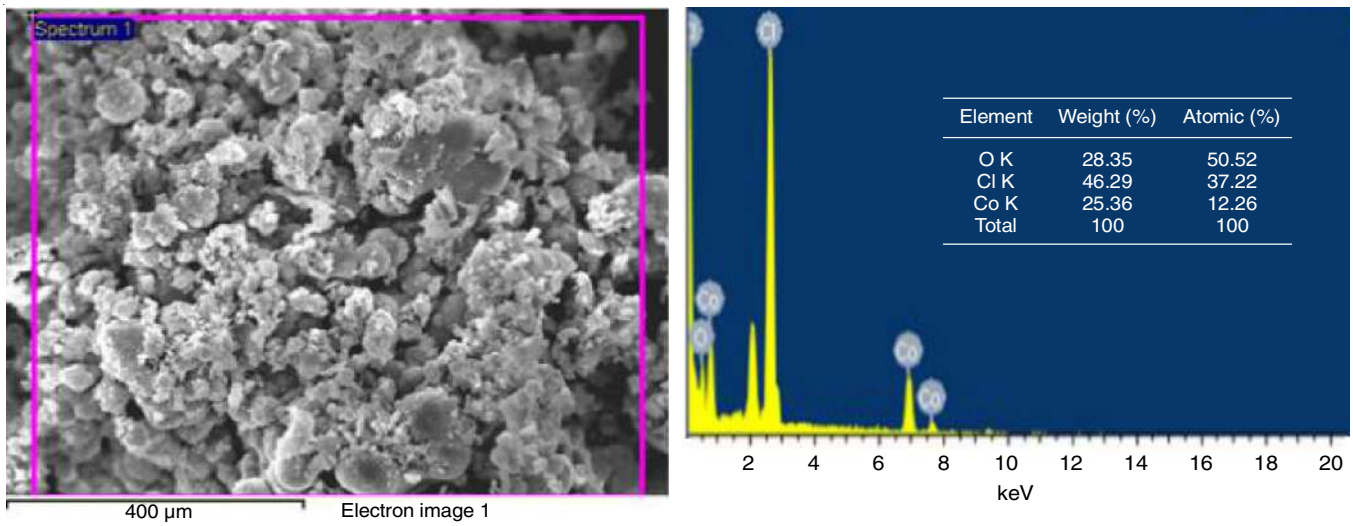

Fig. 6. SEM and EDS of $[Co_2LCl_2(H_2O)_6]$

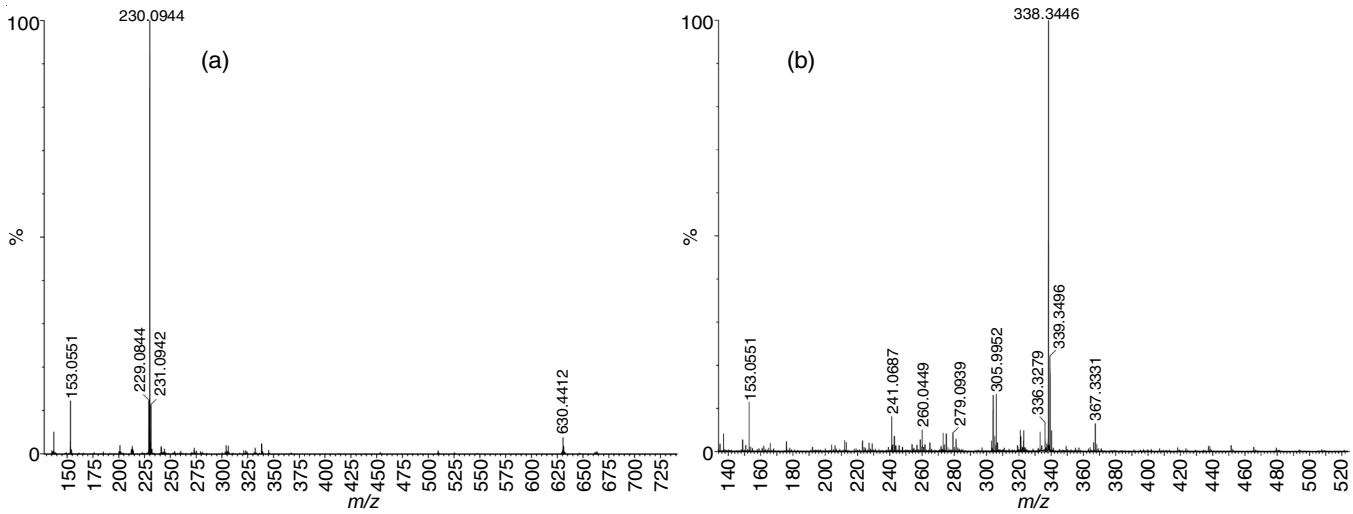

Fig. 7. ESI MS of (a) LH_2 and (b) $[Ni_2LCl_2(H_2O)_6]$

at *m/z* 230.09 likely due to the loss of CH_3 groups, whereas the peak at *m/z* 229.08 is attributed to the loss of carbonyl group [34]. The ESI-MS spectra of Ni(II) complex displayed at *m/z* 339.97 according to its molecular mass (Fig. 7b). The peak at *m/z* 338.3 is attributed to the elimination of CO_2 and H_2O molecules, whereas the signal at *m/z* 260 is due to the removal of the O_2 molecule. The peak at *m/z* 241.1 may result from the elimination of ethylene oxide [35].

XRD: The XRD (powder) spectrum of $Zn_2LCl_2(H_2O)_2$ complex (Fig. 8) and its parameters were evaluated by using LSUCRPC software. The density of complex was measured by using flotation method in separate saturated solutions of benzene, sodium chloride and potassium bromide. By following eqn. 5, the unit cell (n) was calculated;

$$n = \frac{dNV}{M} \quad (5)$$

where d = density; N = Avogadro's number; V = volume; and and M = molecular weight.

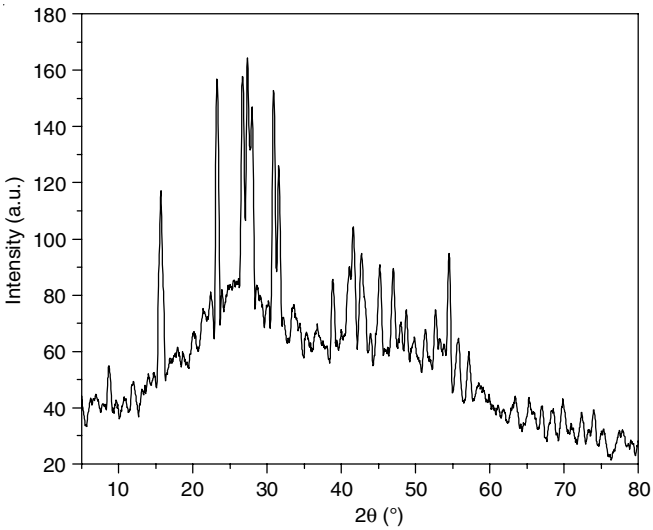

Fig. 8. XRD image of $[Zn_2LCl_2(H_2O)_2]$

From the calculation, the value of n is found to be 2.7 which suggests that the zinc complex exhibits an amorphous nature. The average size of the particle of zinc complex, is 8.9 nm, which was derived from the diffraction pattern of broadening peak by following Debye-Scherrer's equation:

$$D = \frac{K\lambda}{\beta\cos\theta}$$

where D = particle size, K = Scherrer constant, λ = wavelength, β = full width at half maximum at diffraction angle (θ).

Based on the physico-chemical and spectroscopic characterization results, the suggested structure of the synthesized metal complexes are as follows:

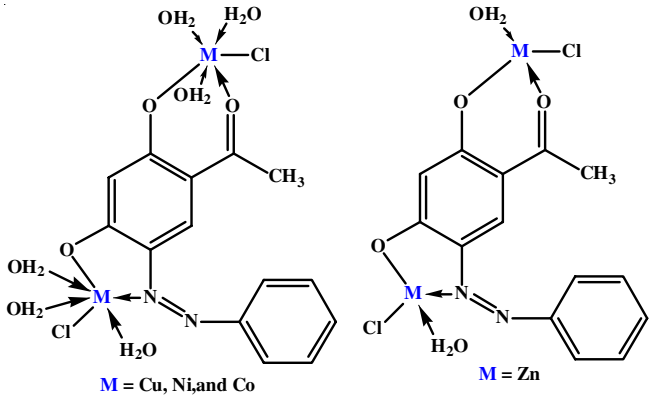

***In vitro* anticancer activity:** The concentration levels at which half of the greatest effect is recorded (IC_{50}) are shown in Table-3. The synthesized Ni(II) and Co(II) complexes exhibited the highest activity against HePG 2 and MCF 7 cancer cell lines (IC_{50} = 13.48 and 17.84 µg/mL at 48 h). Whereas the Co(II) and Ni(II) complexes exhibited moderate activity against liver and breast cancer cell lines (IC_{50} = 19.67 and 14.42 µg/mL at 48 h) and percentage of inhibition explained in Fig. 9. In comparison to other complexes, azo-ligand show the least activity against both the cell lines. These results exemplified how alterations in the chelation molecular structure could result in significant variations in anticancer efficacy.

***In vitro* antioxidant activity:** The DPPH test was used to assess the antioxidant activity of ascorbic acid, azo-ligand LH_2 and the metal complexes (Cu^{2+}, Ni^{2+}, Zn^{2+}, Co^{2+}) at different concentration (5, 10, 15, 20 and 25 µg/mL). The DPPH radical scavenging activity increased concentration-dependently in all samples. Ascorbic acid showed the strongest antioxidant activity, with a maximal inhibition of 78% at 25 µg/mL and an IC_{50} value of 6.81 µg/mL, showing the substantial free radical scavenging ability (Table-4). The Cu(II) complex had the highest activity (IC_{50} = 13.38 µg/mL), followed by Zn(II), Ni(II) and Co(II). The LH_2 had the lowest antioxidant activity (IC_{50} = 34.57 µg/mL), indicating that metal ion complexation improves antioxidant capabilities. Metal complexes, particularly Cu(II), can serve as potent antioxidants by stabilizing free radicals and engaging in redox reactions to neutralize oxidative species.

TABLE-3
IC_{50} VALUE AGAINST MCF-7 AND HEPG-2 CELL LINES

Samples	MCF 7 (IC_{50} in µg/mL)		HepG 2 (IC_{50} in µg/mL)	
	24 h	48 h	24 h	48 h
LH_2	34.19 ± 2.14	24.19 ± 2.94	35.16 ± 4.86	32.34 ± 5.45
Ni(II)	19.47 ± 1.22	14.42 ± 1.10	18.76 ± 1.21	17.84 ± 2.31
Co(II)	17.84 ± 1.09	13.48 ± 1.04	20.84 ± 1.87	19.67 ± 2.98
Zn(II)	27.63 ± 2.98	15.63 ± 1.73	28.48 ± 3.06	25.48 ± 4.03
Cu(II)	31.36 ± 2.47	17.36 ± 1.97	24.42 ± 1.89	22.39 ± 3.85
Doxorubicin	15.51 ± 1.12	10.31 ± 0.12	13.96 ± 1.14	11.66 ± 1.48

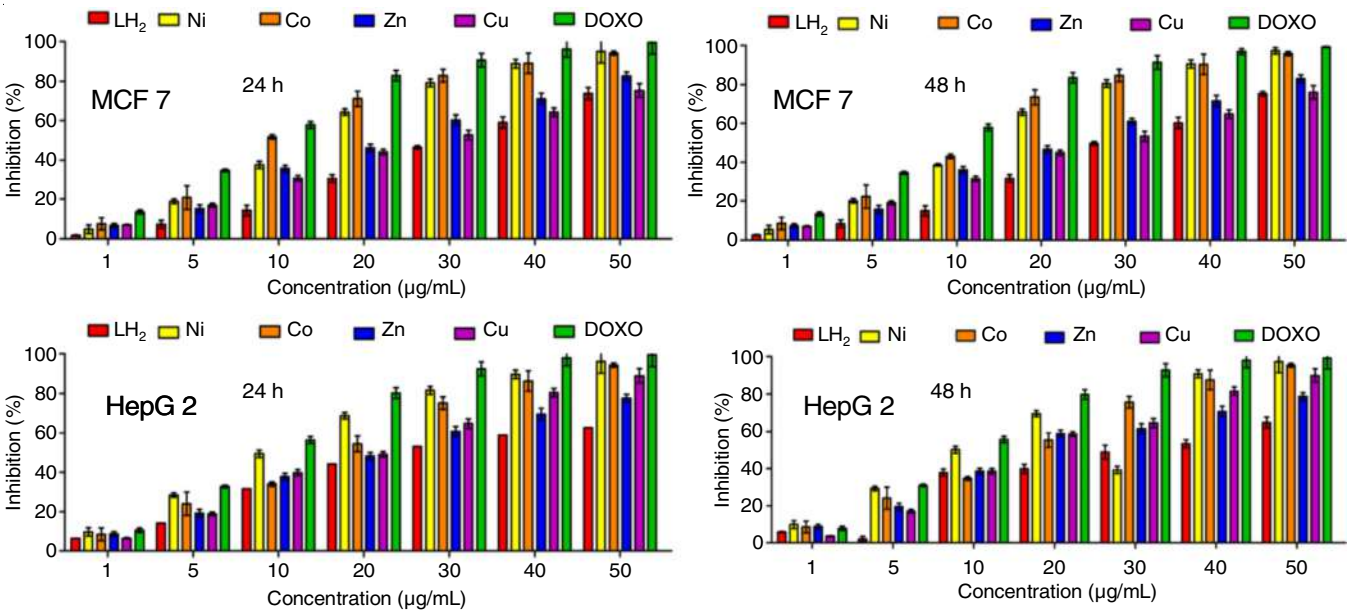

Fig. 9. Percentage of inhibition of ligand and its metal complexes

TABLE-4
PERCENTAGE OF INHIBITION

Conc. (µg/mL)	AA	LH_2	Cu(II)	Ni(II)	Zn(II)	Co(II)
5	46	10	24	20	28	23
10	54	16	47	38	41	33
15	67	22	58	52	49	41
20	73	29	68	59	60	47
25	78	38	72	66	69	52

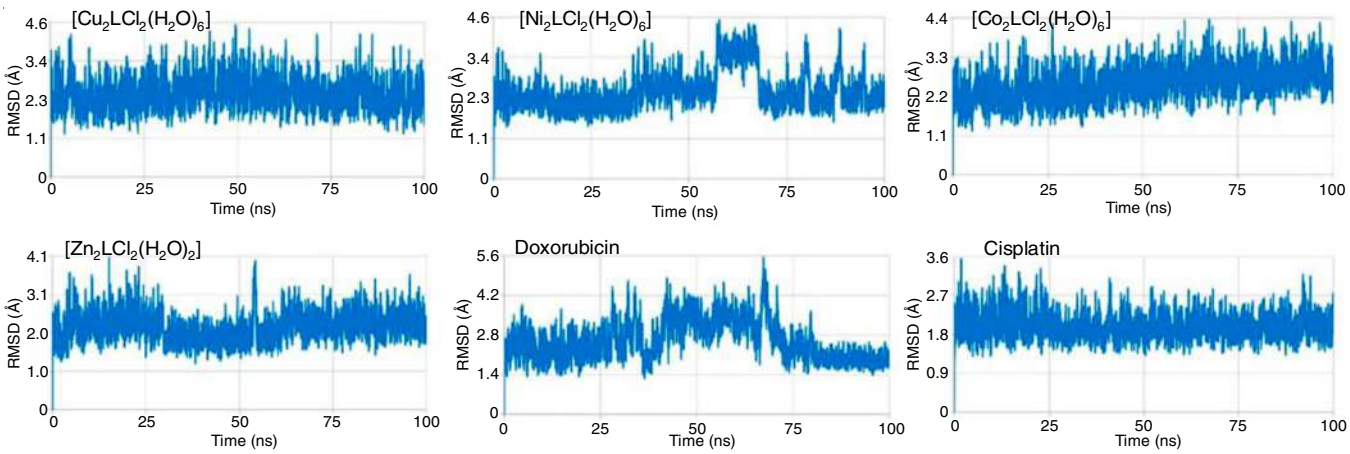

Fig. 10. RMSD graph of complex with doxorubicin and cisplatin

TABLE-5
RMSD AND RMSF VALUE OF METAL COMPLEXES, DOXORUBICIN AND CISPLATIN

Sample	RMSD (Å) (Backbone)			RMSF (Å) (Backbone)		
	100 ns			100 ns		
	Minimum	Maximum	Average	Minimum	Maximum	Average
Cu(II)	1.04	4.51	2.48	1.13	2.16	1.47
Ni(II)	1.20	4.52	2.51	1.12	2.30	1.57
Co(II)	1.07	4.34	2.57	1.13	3.01	1.57
Zn(II)	1.13	4.05	2.21	1.16	2.78	1.55
Doxorubicin	1.09	5.52	2.60	1.25	2.92	1.74
Cisplatin	1.15	3.54	2.00	1.06	1.89	1.33

MD simulations: The initial MD simulation offered a brief description of the ligand-protein complexes stability and interaction patterns. The key metrics of simulation include RMSD (root mean square deviation), RMSF (root mean square fluctuation) and MM-GBSA binding free energy [36]. These criteria were crucial in assessing the efficacy of each ligand in sustaining stable and robust connections with the target protein.

The RMSD assesses the overall stability of the backbone atoms of a molecule throughout the simulation as illustrated in Fig. 10. Lower numbers indicate that the structure is closer to its original shape, implying better stability (Table-5). The minimum deviation measured during the simulation ranged from 1.04 Å Cu(II) to 1.20 Å Ni(II). The highest deviation was detected indicating the most significant structural alterations. The values vary from 3.54 Å (cisplatin) to 5.52 Å (doxorubicin). The Cu(II)to Zn(II)complexes exhibit consistent stability, with average RMSD values ranging from 2.21 Å to 2.57 Å. Cisplatin has the lowest average RMSD (2.00 Å), indicating it retains structural integrity better than doxorubicin (2.60 Å). RMSF assesses the flexibility of individual residues or areas throughout the simulation, with larger values suggesting greater flexibility or movement. The smallest fluctuation in the simulation ranged from 1.06 Å (cisplatin) to 1.25 Å (doxorubicin). The largest fluctuation was observed with the values ranging from 1.89 Å (cisplatin) to 3.01 Å Co(II) and the overall average fluctuation ranges from 1.33 Å (cisplatin) to 1.74 Å (doxorubicin). Cisplatin has the lowest flexibility, with an average RMSF of 1.33 Å and a maximum RMSF of 1.89 Å. Doxorubicin exhibits more flexibility, with a maximum RMSF of 2.92 Å and an average of 1.74 Å (Fig. 11).

Cisplatin exhibits the most stable backbone conformation, the lowest average RMSD (2.00 Å), whereas doxorubicin deviates significantly from its initial structure. Cisplatin has the lowest flexibility, indicating a more rigid structure. Doxorubicin exhibits increased flexibility and volatility, especially in some backbone areas [37]. The results obtained emphasize the relative stability and flexibility of each compound and complex during the 100 ns molecular dynamics simulation, with cisplatin exhibiting greater structural stability and rigidity and doxorubicin being more flexible.

Molecular docking study: The binding efficacy of individual ligands, including the standard drug estradiol benzoate (E2B), against 17-β-HSD1 was evaluated using molecular docking. The docking scores indicated that all ligands demonstrated binding affinities within the range of -7 to -10 kcal/mol, while the standard drug E2B exhibited a superior docking score of -12.18 kcal/mol, against 17-β-HSD1 (Table-6). Among the tested compounds, azo-ligand LH_2 displayed relatively weaker binding energy compared to its metal-complex counterparts. This suggests that the incorporation of transition metals into the azo-dye ligand significantly enhances their binding efficacy, likely due to the ability of transition metals to modulate electronic properties and improve antiproliferative activity. Among the four synthesized metal(II) complexes, Ni(II) showed the strongest binding affinity with a docking score of -9.81 kcal/mol, while Co(II) demonstrated a comparatively lower binding efficacy with a docking score of -8.22 kcal/mol. The enhanced binding affinity observed for Ni(II) can be attributed to the optimal coordination and electronic properties, which contribute to a more favourable interaction with the target protein.

TABLE-6
DOCKING SCORE OF AZO DYE AND ITS METAL COMPLEXES

Sample	Docking score
LH_2	-7.74
$[Co_2LCl_2(H_2O)_6]$	-8.22
$[Cu_2LCl_2(H_2O)_6]$	-9.30
$[Ni_2LCl_2(H_2O)_6]$	-9.81
$[Zn_2LCl_2(H_2O)_2]$	-8.43
Standard drug (E2B)*	-12.18

Protein-ligand interaction analyses revealed that the ligands formed 3 to 7 hydrogen bonds with 17-β-HSD1, along with other non-covalent interactions, including carbon-hydrogen bonds, van der Waals forces, pi-pi alkyl interactions, pi-sigma interactions and pi-pi stacking. These interactions are consistent with the generated docking scores and highlight the role of specific chemical moieties in stabilizing the ligand-protein complex (Figs. 12 and 13). Remarkably, Ni(II) complex exhibited the highest number of hydrogen bonds, further supporting its stronger binding affinity and higher docking score compared to other ligands.

HOMO-LUMO surface energy analysis: The HOMO, LUMO and their energy gap (ΔE_{H-L}) of the selected ligands were analyzed and are depicted in Fig. 14. The HOMO-LUMO energy plots were visualized to examine the electronic distribution patterns and their implications for binding interactions. The energy gap is a crucial parameter, as it determines the

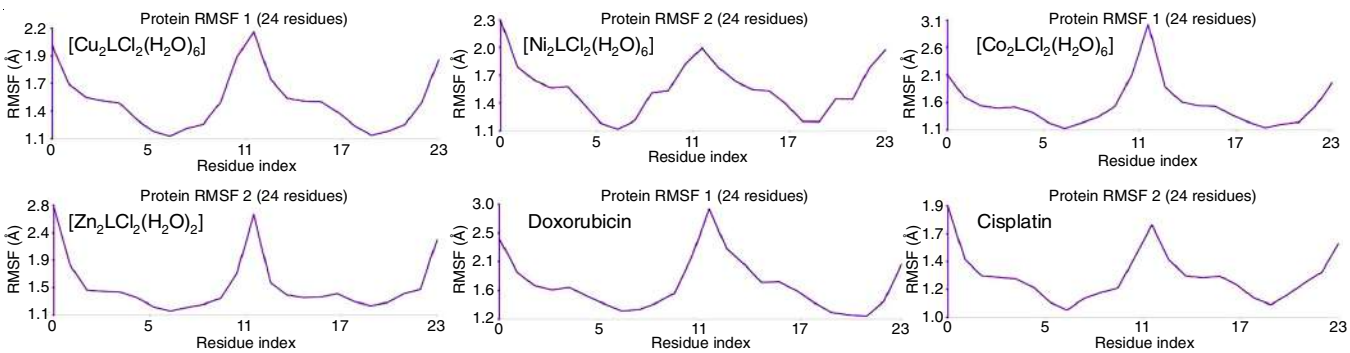

Fig. 11. RMSF graph of complex with doxorubicin and cisplatin

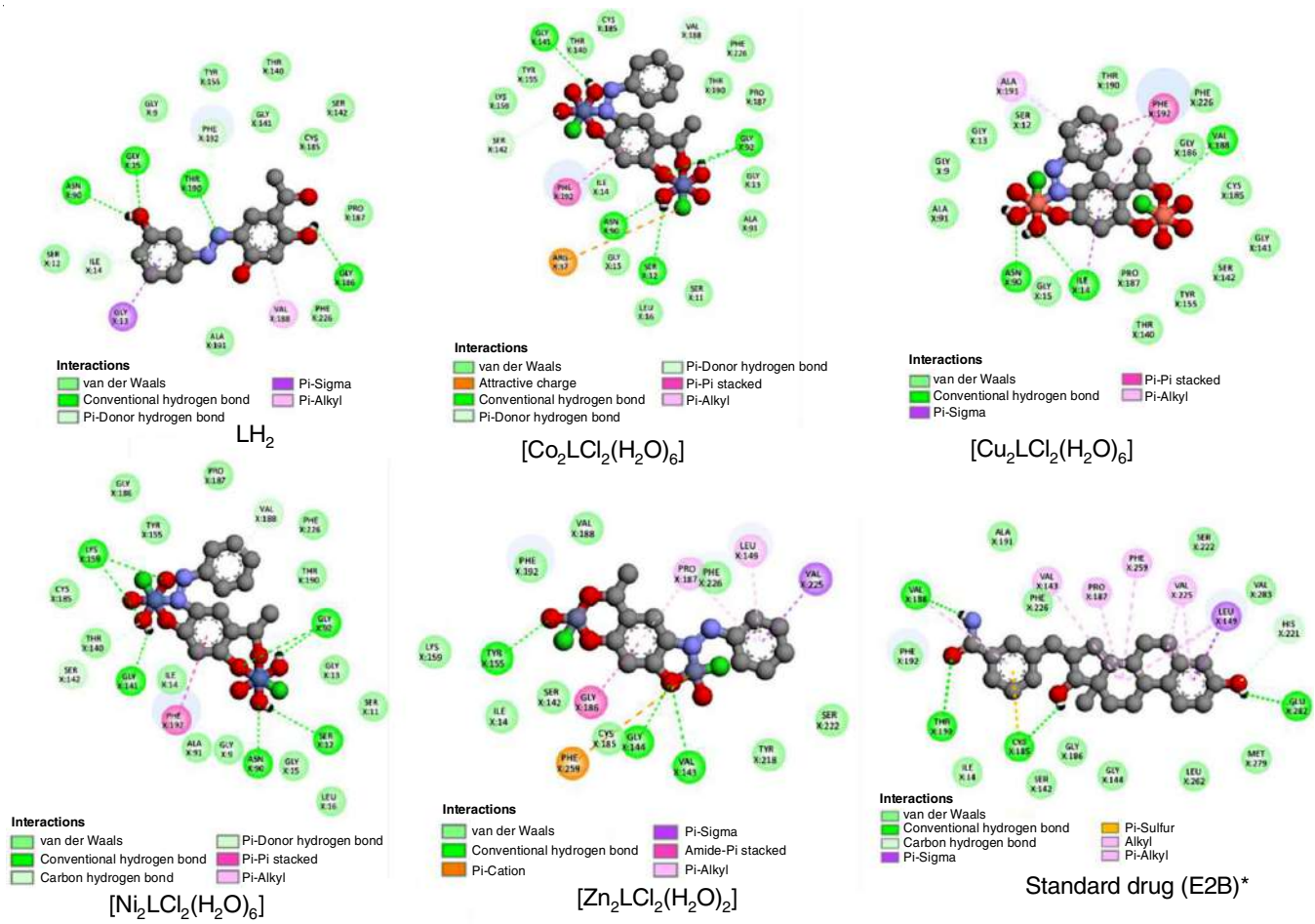

Fig. 12. 2D Image of ligand and its metal complexes including standard drug (E2B)* with 3hb5 protein

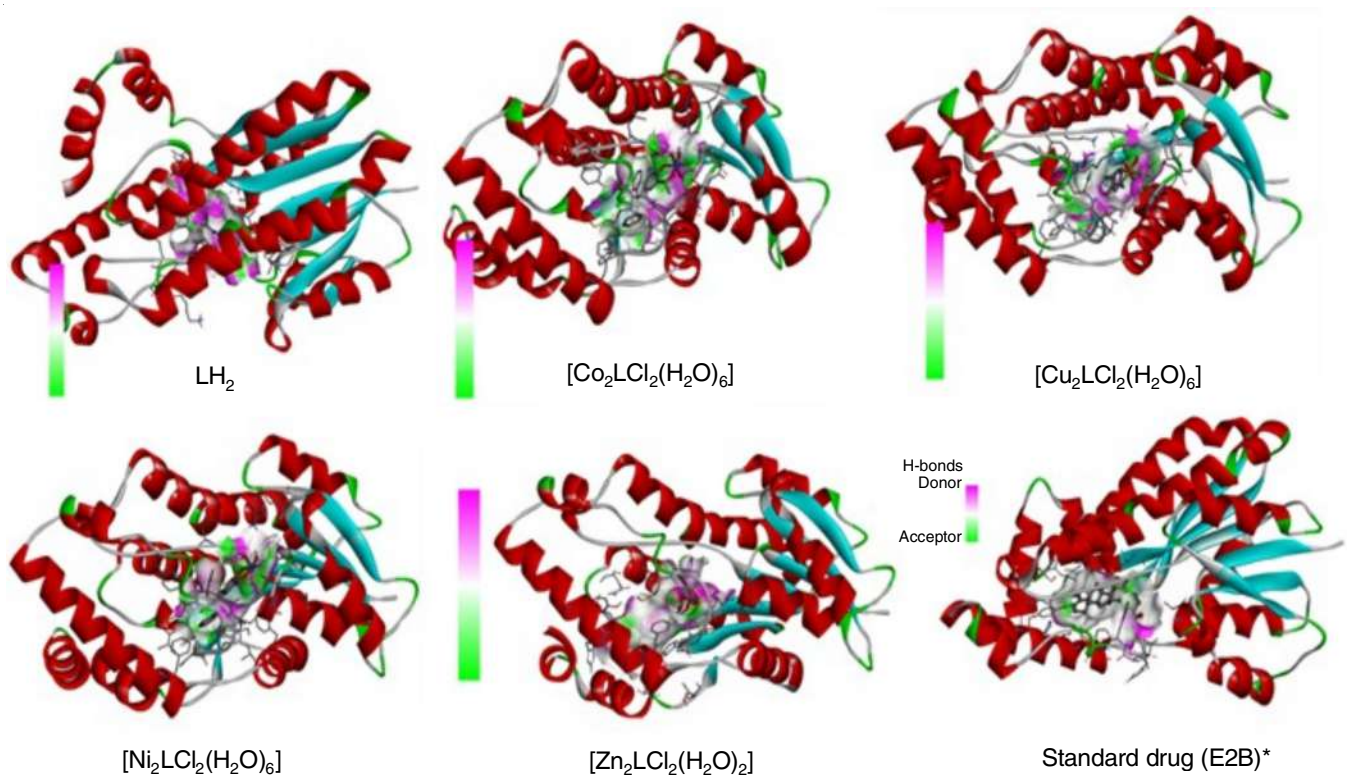

Fig. 13. 3D Image of ligand and its metal complexes including standard drug (E2B)* with 3hb5 protein

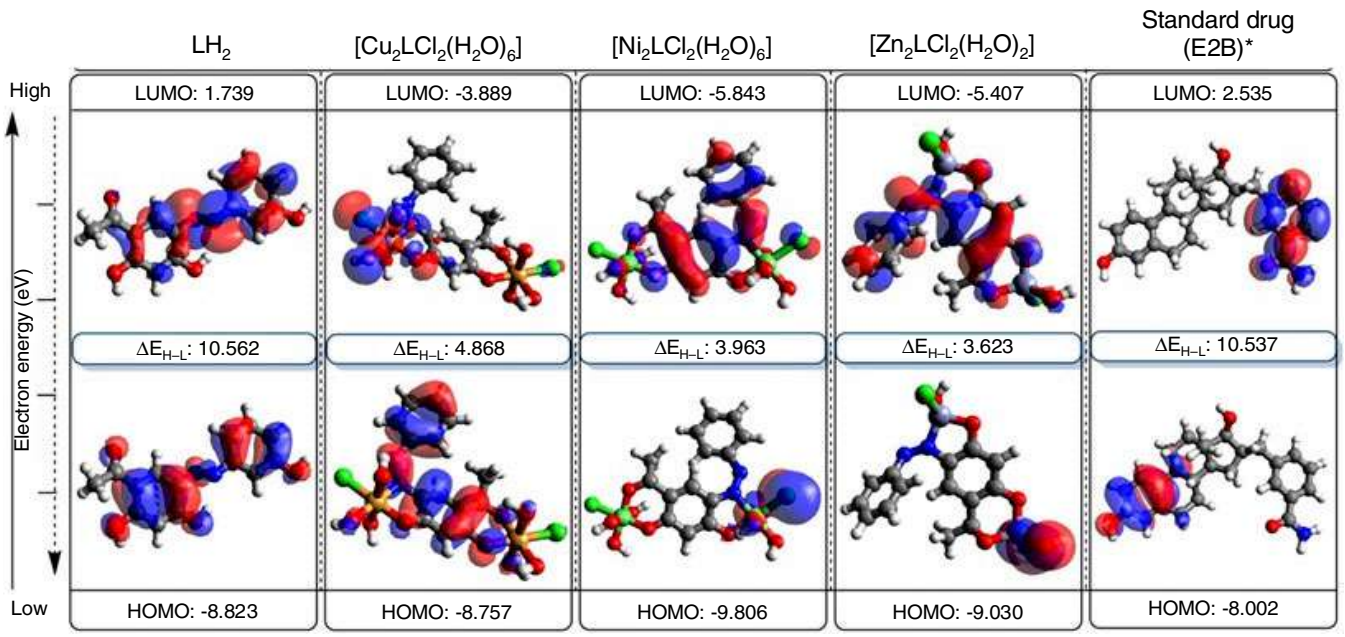

Fig. 14. The HOMO, LUMO and their energy gap (ΔE_{H-L}) of proposed ligands along with standard drug during analyzing their flexibility and stability in an orbital theory prospective

TABLE-7
PHARMACOKINETIC STUDY OF METAL COMPLEXES

Molecule	MW (g/mol)	log P	GIA	HBA	HBD	LR	BS	SA	BBB	PgP substrate
Cu(II)	456.27	3.08	High	5	2	Yes	0.55	2.68	Yes	Yes
Ni(II)	446.57	3.08	High	5	2	Yes	0.55	2.68	Yes	No
Co(II)	447.04	3.08	High	5	2	Yes	0.56	2.69	No	No
Zn(II)	447.04	3.08	High	5	2	Yes	0.55	2.69	No	No

MW: Molecular weight, HBA: H-bond acceptors, HBD: H-bond donors, GIA: GI absorption, BBBP: BBB permeant, LV: Lipinski violations, BS: Bioavailability Score, SA: Synthetic accessibility.

chemical stability and reactivity of the ligands. Among the analyzed ligands, the standard drug E2B exhibited the highest energy gap (10.537 eV), which was comparable to that of the non-metal ligand LH_2 (10.562 eV), indicating high kinetic stability and low reactivity. In contrast, the metal(II) complex displayed significantly lower energy gaps, ranging between 3 to 5 eV, signifying greater reactivity. Specifically, Ni(II) complex exhibited an energy gap of 3.963 eV, Zn(II) complex had 3.623 eV and Cu(II) complex showed 4.868 eV. The reduced energy gaps of these metal-based ligands highlight their potential for enhanced interaction with the target protein due to their higher reactivity.

ADME studies: Table-7 depicts the ADME properties for four azo based metal(II) complexes. The log P value shows the lipophilicity of molecule (ability to dissolve in fats *versus* water). A log P of 3.08 shows considerable lipophilicity, which promotes absorption and permeability. All the compounds demonstrate a significant GIA, suggesting they are effectively absorbed through the gastrointestinal tract. Each molecule possesses 5 hydrogen bond acceptors (HBA) and 2 hydrogen bond donors (HBD), which falls well within Lipinski's rule of five for drug-likeness. The compounds match the drug-likeness criteria (molecular weight < 500 g/mol, log P < 5, HBA ≤ 10, HBD ≤ 5). Each chemical has a bioavailability score of 0.55, indicating a moderate oral bioavailability. The synthetic accessibility (SA) ratings varied from 2.68 to 2.69, indicating that these compounds are generally simple to synthesize (on a scale where lower values are preferred). Molecules Cu(II) and Ni(II) can cross the blood-brain barrier (BBB), whereas Co(II) and Zn(II) cannot. Molecule Cu(II) is a P-glycoprotein (PgP) substrate, which means it can be expelled from cells *via* PgP transport, potentially affecting the medication retention and efficacy. Ni(II) is not a PgP substrate, while Co(II) and Zn(II) are similarly non-substrates, implying that these molecules are less likely to be actively eliminated by cells.

All the synthesized azo-based metal(II) compounds follow to Lipinski's rule of five, suggesting they possess characteristics typical of drugs and are probably suitable for oral administration. Cu(II) and Ni(II) exhibit a stronger tendency to penetrate the blood-brain barrier (BBB), potentially positioning them as suitable candidates for neurological applications. In contrast, Co(II) and Zn(II) lack BBB permeability, indicating a higher likelihood of targeting peripheral organs. Cu(II) and Ni(II) have good BBB penetration and GIA, however only Cu(II) is PgP substrate [38]. All compounds exhibit good drug-like qualities, including no Lipinski's violations, high gastrointestinal absorption and moderate bioavailability. The synthetic accessibility scores indicate that they are quite easy to construct.

Conclusion

This study demonstrated the successful synthesis and characterization of a novel azo-dye ligand (LH_2) and its metal complexes, revealing their enhanced bioactivities upon complexation with Cu(II), Ni(II), Co(II) and Zn(II). The antioxidant properties of the Cu(II) complex and the cytotoxic potential of the Ni(II) and Co(II) complexes against MCF-7 and HepG2 cell lines establish these compounds as promising candidates for therapeutic development. The strong antioxidant and anticancer activities can be attributed to the synergistic interactions between the azo ligand and the metal ions, as evidenced by detailed spectroscopic, thermal and computational analyses. Molecular docking and dynamic simulations not only validated the binding efficiency of these complexes but also revealed key electronic and structural properties essential for their biological performance. The Cu(II) and Ni(II) complexes displayed favourable ADME characteristics, supporting their potential for further exploration in drug development pipelines. Overall, the study highlights the versatility of azo-metal complexes in biomedical applications. Future work should focus on *in vivo* evaluations, comprehensive toxicity studies and exploring structure-activity relationships to optimize these compounds for clinical uses.

ACKNOWLEDGEMENTS

The authors are grateful to NISER, Bhubaneswar, for providing spectral analysis (NMR, ESI-MS, XRD and ESR) of synthesized compounds.

CONFLICT OF INTEREST

The authors declare that there is no conflict of interests regarding the publication of this article.

REFERENCES

1. S. Benkhaya, S. M'rabet and A. El Harfi, *Heliyon*, **6**, e03271 (2020); https://doi.org/10.1016/j.heliyon.2020.e03271
2. D.P. Mishra, P.K. Sahu, B. Acharya and S.K. Ranajit, *Bionanoscience*, **14**, 3693 (2024); https://doi.org/10.1007/s12668-024-01513-x
3. R. Kilincarslan, E. Erdem and H. Kocaokutgen, *Transition Met. Chem.*, **32**, 102 (2007); https://doi.org/10.1007/s11243-006-0134-x
4. D.P. Mishra, P.K. Sahu, B. Acharya, S.P. Mishra and S. Bhati, *Results Chem.*, **10**, 101712 (2024); https://doi.org/10.1016/j.rechem.2024.101712
5. M.N. Khan, D.K. Parmar and D. Das, *Mini-Rev. Med. Chem.*, **21**, 1071 (2021); https://doi.org/10.2174/1389557520999201123210025
6. S.H. Jawad and K.J. Al-Adilee, *J. Mol. Struct.*, **1277**, 134846 (2023); https://doi.org/10.1016/j.molstruc.2022.134846
7. H. Mohammed, A. Sultan, W. Ali Eltayb, U. O. Edet, E. Aniebo Umoh and M. Abdalla, *Bull. Chem. Soc. Ethiop.*, **39**, 287 (2025); https://doi.org/10.4314/bcse.v39i2.8
8. A.A. Noser, A.-A.-B. Alkhikany, M.M. Salem and H.A.A.E. Salam, *J. Mol. Struct.*, **1323**, 140783 (2025); https://doi.org/10.1016/j.molstruc.2024.140783
9. G.Y. Akarsh, M.N. Manjunatha, B.S. Krishna, H.A. Anilkumara, N. Ranjitha, N.K. Vasantakumarnaik and G. Krishnamurthy, *J. Mol. Struct.*, **1322**, 140448 (2025); https://doi.org/10.1016/j.molstruc.2024.140448
10. A. Oveisi-Keikha, S. Shahraki, E. Dehghanian and H. Mansouri-Torshizi, *Spectrochim. Acta A*, **325**, 125034 (2025); https://doi.org/10.1016/j.saa.2024.125034
11. P. Skehan, R. Storeng, D. Scudiero, A. Monks, J. McMahon, D. Vistica, J.T. Warren, H. Bokesch, S. Kenney and M.R. Boyd, *J. Natl. Cancer Inst.*, **82**, 1107 (1990); https://doi.org/10.1093/jnci/82.13.1107
12. W.H. Mahmoud, F.N. Sayed and G.G. Mohamed, *Appl. Organomet. Chem.*, **30**, 959 (2016); https://doi.org/10.1002/aoc.3529
13. D.Y. Fnfoon and K.J. Al-Adilee, *J. Mol. Struct.*, **1271**, 134089 (2023); https://doi.org/10.1016/j.molstruc.2022.134089
14. W.H. Mahmoud, F.N. Sayed and G.G. Mohamed, *Appl. Organomet. Chem.*, **32**, 4347 (2018); https://doi.org/10.1002/aoc.4347
15. K.J. Al-Adilee and H.M. Hessoon, *J. Phys. Conf. Ser.*, **1234**, 012094 (2019); https://doi.org/10.1088/1742-6596/1234/1/012094
16. Y. Kumar, N.K. Singh, V.D. Singh, I. Ali, R.K. Tiwari, A. Kumar and D.S. Pandey, *Inorg. Chim. Acta*, **538**, 120963 (2022); https://doi.org/10.1016/j.ica.2022.120963
17. Y.J. Sahar and H.S. Mohammed, *Al-Qadisiyah J. Pure Sci.*, **24**, 32 (2019).
18. A.M. Khedr, A.A. Gouda and H.A. El-Ghamry, *J. Mol. Liq.*, **352**, 118737 (2022); https://doi.org/10.1016/j.molliq.2022.118737
19. E. Bursal, A. Aras and Ö. Kiliç, *Nat. Prod. Res.*, **33**, 1975 (2019); https://doi.org/10.1080/14786419.2018.1480018
20. L.H. Madkour, S. Kaya, L. Guo and C. Kaya, *J. Mol. Struct.*, **1163**, 397 (2018); https://doi.org/10.1016/j.molstruc.2018.03.013
21. L.H. Madkour, S. Kaya, C. Kaya and L. Guo, *J. Taiwan Inst. Chem. Eng.*, **68**, 461 (2016); https://doi.org/10.1016/j.jtice.2016.09.015
22. K. Binder, J. Horbach, W. Kob, W. Paul and F. Varnik, *J. Phys. Condens. Matter*, **16**, S429 (2004); https://doi.org/10.1088/0953-8984/16/5/006
23. N. MichaudAgrawal, E.J. Denning, T.B. Woolf and O. Beckstein, *J. Comput. Chem.*, **32**, 2319 (2011); https://doi.org/10.1002/jcc.21787
24. M.R. Islam, J.Z. Tayyeb, H.K. Paul, M.N. Islam, G.O. Oduselu, I. Bayýl, M.H. Abdellattif, K.M. Al-Ahmary, S.R. Al-Mhyawi and M.E.A. Zaki, *J. Cell. Mol. Med.*, **28**, e18584 (2024); https://doi.org/10.1111/jcmm.18584
25. S.S. Swain, S.R. Singh, A. Sahoo, P.K. Panda, T. Hussain and S. Pati, *Proteins*, **90**, 1617 (2022); https://doi.org/10.1002/prot.26341
26. L.M. Ramorobi, G.R. Matowane, S.S. Mashele, S.L. Bonnet, A.E.M. Noreljaleel, S.S. Swain, T.J. Makhafola and C.I. Chukwuma, *J. Food Biochem.*, **46**, e14360 (2022); https://doi.org/10.1111/jfbc.14360
27. Š. Staršèevic, S. Turk, B. Brus, J. Cesar, T. Lanišnik Ri•ner and S. Gobec, *J. Steroid Biochem. Mol. Biol.*, **127**, 255 (2011); https://doi.org/10.1016/j.jsbmb.2011.08.013
28. Y.F. Qiao, L. Du, J. Zhou, Y. Hu, L. Li, B. Li and Q.H. Zhao, *J. Coord. Chem.*, **67**, 2615 (2014); https://doi.org/10.1080/00958972.2014.948870
29. E.S. Freeman and B. Carroll, *J. Phys. Chem.*, **62**, 394 (1958); https://doi.org/10.1021/j150562a003
30. C. Anitha, S. Sumathi, P. Tharmaraj and C.D. Sheela, *Int. J. Inorg. Chem.*, **2011**, 493942 (2011); https://doi.org/10.1155/2011/493942
31. P.S. Jogi, J. Meshram, J. Sheikh and T.B. Hadda, *Med. Chem. Res.*, **22**, 4202 (2013); https://doi.org/10.1007/s00044-012-0421-3
32. M.A. Pujante-Galián, S.A. Pérez, M.G. Montalbán, G. Carissimi, M.G. Fuster, G. Víllora and G. García, *Molecules*, **25**, 5063 (2020); https://doi.org/10.3390/molecules25215063
33. T.A. Yousef, G.M.A. El-Reash, T.H. Rakha and U. El-Ayaan, *Spectrochim. Acta A Mol. Biomol. Spectrosc.*, **83**, 271 (2011); https://doi.org/10.1016/j.saa.2011.08.030
34. N. Nishat, Rahisuddin, M.M. Haq and V. Kumar, *J. Coord. Chem.*, **59**, 1729 (2006); https://doi.org/10.1080/00958970600611673
35. H. Khanmohammadi, K. Rezaeian, M.M. Amini and S.W. Ng, *Dyes Pigments*, **98**, 557 (2013); https://doi.org/10.1016/j.dyepig.2013.03.023
36. J.W. Pitera, *J. Phys. Chem. B*, **118**, 6526 (2014); https://doi.org/10.1021/jp412776d
37. C. Chen and H. Yang, *J. Opt. Soc. Am. A Opt. Image Sci. Vis.*, **34**, 2070 (2017); https://doi.org/10.1364/JOSAA.34.002070
38. F.X. Domínguez-Villa, N.A. Durán-Iturbide and J.G. Ávila-Zárraga, *Bioorg. Chem.*, **106**, 104497 (2021); https://doi.org/10.1016/j.bioorg.2020.104497